







The regulatory role of CARBON STARVED ANTHER-mediated photoperiod-dependent male fertility in rice

Jingbin Li,¹ Duoxiang Wang ,¹ Shiyu Sun ,¹ Linlin Sun,¹ Jie Zong,¹ Yaqi Lei,¹ Jing Yu,¹ Wanqi Liang  and Dabing Zhang ^{1,2,*,*†}

1 Joint International Research Laboratory of Metabolic and Developmental Sciences, State Key Laboratory of Hybrid Rice, School of Life Sciences and Biotechnology, Shanghai Jiao Tong University, Shanghai, China

2 School of Agriculture, Food and Wine, University of Adelaide, Urrbrae, Australia

*Author for correspondence: zhangdb@sjtu.edu.cn

†Senior author

D.Z. and W.L. conceived and designed the research. J.L., D.W., L.S., and Y.L. performed the experiments. J.Y. and D.Z. supervised the experiments. J.L. analyzed the data and wrote the article. S.S. and J.Z. provided technical assistance to data analysis. D.Z. supervised and completed the writing.

The author responsible for distribution of materials integral to the findings presented in this article in accordance with the policy described in the Instructions for Authors (<https://academic.oup.com/plphys/pages/general-instructions>) is: Dabing Zhang (zhangdb@sjtu.edu.cn).

Abstract

Environmental signals, especially daylength, play important roles in determining fertility in photoperiod-sensitive genic male sterile (PGMS) lines that are critical to sustain production of high-yielding hybrid rice (*Oryza sativa*) varieties. However, the mechanisms by which PGMS lines perceive changes in photoperiod and transmit those signals to elicit downstream effects are not well understood. In this study, we compared the transcriptomes from the leaves and anthers of *carbon starved anther* (*csa*), a PGMS line, to wild-type (WT) tissues under different photoperiods. Components of circadian clock in the leaves, including *Circadian Clock-Associated 1* and *Pseudo-Response Regulator* (*PRR95*), played vital roles in sensing the photoperiod signals. Photoperiod signals were weakly transduced to anthers, where gene expression was mainly controlled by the *CSA* allele. *CSA* played a critical role in regulating sugar metabolism and cell wall synthesis in anthers under short-day conditions, and transcription of key genes inducing *csa*-directed sterility was upregulated under long-day (LD) conditions though not to WT levels, revealing a mechanism to explain the partial restoration of fertility in rice under LD conditions. Eight direct targets of *CSA* regulation were identified, all of which were genes involved in sugar metabolism and transport (cell wall invertases, SWEETs, and monosaccharide transporters) expressed only in reproductive tissues. Several hub genes coordinating the effects of *CSA* regulation were identified as critical elements determining WT male fertility and further analysis of these and related genes will reveal insights into how *CSA* coordinates sugar metabolism, cell wall biosynthesis, and photoperiod sensing in rice anther development.

Introduction

Hybrid vigor (heterosis), a universal phenomenon in crops, increases grain yields by crossing two genetically distinct elite parental lines. Grain yield in rice (*Oryza sativa* L.) has

increased substantially since the advent of male-sterile lines, which facilitate the production of hybrid varieties (Cheng et al., 2007). More recently, the development of lines whose sterility can be controlled by environmental factors, such as

daylength or temperature, has further simplified rice breeding (Shi, 1985). Since the 1990s, photoperiod-sensitive genic male sterile (PGMS) rice lines have emerged as a crucial tool in rice breeding, as daylength is much more predictable than temperature or humidity. Numerous loci that control PGMS traits have been cloned, especially in the most widely used PGMS line, Nongken58S (Zhang et al., 1994; Mei, 1999; Ding et al., 2012; Zhou et al., 2012; Fan et al., 2016). While two genetic loci directing PGMS in this line are known, the underlying molecular mechanisms in regulating the male fertility in response to photoperiod for the two independent loci remain unclear.

Plants possess an internal biological clock that responds to fluctuations in daylength to anticipate seasonal changes; response to photoperiod is mediated by complex interactions between environmental signals and the endogenous circadian clock (Hayama and Coupland, 2003). The circadian clock has an approximately 24 h period, composed of three main parts: input, the central oscillator, and output (Dunlap, 1999). Light and temperature signals (the input) are conveyed to the central oscillator, which is composed of multiple factors organized in interlocked transcriptional and posttranslational feedback loops. In *Arabidopsis thaliana*, genes encoding two MYB transcription factors, *Circadian Clock-Associated 1* (CCA1) and *Late Elongated Hypocotyl* (LHY), are expressed in the early morning and repress the evening-phased gene *Timing of Cab Expression 1* (TOC1, also known as PRR1) (Alabadi et al., 2001). Three members of pseudo-response regulator (PRR) gene family (PRR9, PRR7, and PRR5) are expressed sequentially during the day, and in turn repress CCA1 and LHY transcription (Nakamichi et al., 2010). At dusk, TOC1 is induced as levels of CCA1 and LHY decrease. In the night, the evening complex (EC), formed from proteins encoded by *Lux Arrhythmo* (LUX), *Early Flowering 3* (ELF3), and *ELF4*, promotes expression of the two morning factors, CCA1 and LHY, which in turn repress the three components of EC (Nagel and Kay, 2013; Adams et al., 2015). In addition, CCA1 and LHY can repress their own transcription by binding to their own, and each other's, promoters (Adams et al., 2015).

The clock-related components have been reported to be highly conserved in rice (Murakami et al., 2003, 2007). CCA1 is the only ortholog of *Arabidopsis* LHY/CCA1 (Murakami et al., 2007; Sun et al., 2021a). In addition, five members of the PRR family (PRR1, PRR37, PRR73, PRR59, and PRR95) have been identified as rice putative orthologs of *Arabidopsis* clock-associated genes PRR1, PRR3, PRR7, PRR5, and PRR9 (Murakami et al., 2003, 2007). Two rice orthologs of ELF3 have also been identified: *ELF3-1* is required for heading date control under long-day (LD) conditions by affecting the expression of clock-related genes including PRR1, PRR95, PRR73, PRR37, and PRR59 (Yang et al., 2013); while *ELF3-2/EF3* regulates heading date by influencing the basic vegetative growth period stage instead of photoperiodic sensitivity (Fu et al., 2009).

Circadian clock helps optimize plant growth and development such as flowering bud break, and the onset of senescence and dormancy (Malapeira et al., 2014; Flis et al., 2016). In *Arabidopsis*, flowering time is controlled by the GIGANTEA (GI)–CONSTANS (CO)–FLOWERING LOCUS T (FT) pathway, where GI is involved in phytochrome signaling to activate CO, a transcription factor that in turn activates FT, a flowering hormone (florigen) (Putterill et al., 1995). In rice, Heading date 1 (Hd1), an ortholog of CO (Yano et al., 2000), acts upstream of two florigens, Hd3a and Rice Flowering Locus 1 (RFT1), which are orthologs of FT (Sun et al., 2014). Under short-day (SD) conditions, a GI–Hd1–Hd3a pathway in rice, similar to that in *Arabidopsis*, induces flowering; rice also has a second transcription factor, Early Hd1 (Ehd1), with no ortholog in *Arabidopsis*, that activates both *Hd3a* and *RFT1* expression (Sun et al., 2014). However, under LD conditions, Hd1 represses expression of *Hd3a* (Sun et al., 2014), so rice flowering is induced via the Ehd1–RFT1 pathway (Doi et al., 2004).

As male fertility is crucial for hybrid rice breeding, understanding the molecular mechanisms of rice anther and pollen development is a core requirement for developing new male sterile lines (Zhang and Wilson, 2009). As nonphotosynthetic sink tissues, plant anther requires a supply of carbohydrates, usually in the form of sucrose transported via the phloem from source tissues (flag leaves), to support pollen development and maturation (Turgeon and Wolf, 2009; Zhang and Wilson, 2009; Bihmidine et al., 2013). Sucrose is unloaded from the phloem into the cell wall matrix of sink tissues by Sugars Will Eventually be Exported Transporter (SWEET) proteins; loss of SWEET function results in defective seed filling in maize (*Zea mays*) and rice (Sosso et al., 2015; Yang et al., 2018) and defective microspore development in rice (Chu et al., 2006). Cell wall invertases (CWINs) are typically expressed in sinks to hydrolyze sucrose into glucose and fructose (Ruan, 2014). In rice, CWIN3 (INV4) is a cold-induced transporter of sucrose for pollen cell wall development (Oliver et al., 2005). Monosaccharides, hydrolyzed from sucrose by CWINs, are moved throughout the cell via monosaccharide transporters (MSTs) in angiosperms (Ruan, 2014; Rottmann et al., 2018; Deng et al., 2019). UDP-glucose pyrophosphorylase (UGPase) is also related to sucrose degradation for the metabolic demand of anther and pollen development (Winter and Huber, 2000). Loss of UGPase function leads to new thermosensitive male sterile lines in rice (Chen et al., 2007a).

Carbon starved anther (CSA) is an R2R3 MYB transcription factor that regulates sugar partitioning from photosynthetic tissues (sources) to anthers (sinks) to promote pollen maturation in rice (Zhang et al., 2010). In loss-of-function *csa* mutants, sugars accumulate in source leaves, impairing anther development due to lack of sugar, and resulting in total pollen sterility (Zhang et al., 2010). Further research reported that the *csa* mutant was a PGMS line, sterile under SD conditions but with restored fertility under LD

conditions (Zhang et al., 2013). However, how CSA senses and responds to the photoperiod signals is not clear.

In this study, we describe the effects of photoperiod on gene expression in wild-type (WT) and *csa* flag leaves and anthers to identify putative central factors that transduce photoperiod signals via CSA in both leaves and anthers. By analyzing the co-expression of candidate genes, we dissect the potential mechanisms that: cause *csa*-induced sterility under SD conditions; partially restore fertility in *csa* anthers under LD conditions; and finally, are responsible to restore full WT fertility under LD and SD conditions. We have also verified several downstream target genes directly regulated by CSA that encode important components in sugar metabolism during the anther development.

Results

Photoperiod changes have great effects on gene expression in flag leaves

Leaves are the main plant organs that sense and respond to environmental cues, such as daylength and temperature (Corbesier et al., 2007). To investigate how the PGMS line, *csa*, responds to changes in photoperiod, we sampled flag leaves every 4 h during a 24-h period from WT and *csa* plants grown under SD (12-h light) and LD (14 h) conditions (Supplemental Figure S1). Under these conditions, the WT (WT-SD and WT-LD) plants produce viable pollen, *csa*-SD plants are completely sterile, while *csa*-LD pollen is semi-fertile (Zhang et al., 2013). We performed transcriptome analysis on the four genotype/photoperiod flag leaf combinations at the six timepoints (Supplemental Data set S1). Expression profiles for 6,266 transcripts clustered into 14 groups, all of which were defined by differences between LD and SD photoperiods (Figure 1A and Supplemental Data set S1).

The largest cluster, Cluster 2, contained 1,290 genes that peaked at dawn (ZT23–ZT3) in LD plants, or mid-morning (ZT3–ZT7) in SD plants (Figure 1A). This cluster contained *CCA1*, a core factor of circadian clock rhythm (Murakami et al., 2007); *Rice Dof Daily Fluctuations 1 (RDD1)*, a reported circadian clock- and phytochrome-regulated *Dof*-like gene (Iwamoto et al., 2009); *Ehd1*, involved in rice flowering control (Doi et al., 2004); and two florigen genes, *Hd3a* and *RFT1*, that affect flowering time in response to photoperiod (Doi et al., 2004; Figure 1, B–F). Clusters 3 and 4 contained 759 genes that were highly expressed during the day, but predominantly in either LD or SD plants (Figure 1A): in Cluster 3, *PRR95*, a clock-associated gene (Murakami et al., 2007), was expressed much more highly in SD than in LD plants (Figure 1G), while in Cluster 4, *DNA binding with one finger 12 (DOF12)*, which has been reported as a flowering regulator that controls the expression of *Hd3a* and *MADS14* (Li et al., 2009), was much more highly expressed in LD plants (Figure 1H). Clusters 5, 6, 7, 9, and 10 contained 2,219 genes whose expression peaked at different times from noon to midnight, with a noticeable lag of several hours in SD plants (Figure 1A). Among these, the genes in Cluster 9 exhibited the larger response to photoperiod, being much

more highly expressed in LD plants, and included *Hd1*, an important regulator of flowering in rice (Yano et al., 2000; Figure 1I). Clusters 11, 12, 13, and 14 contained 1,633 genes expressed more highly at nighttime (Figure 1A). In total, 1,067 genes in Clusters 11 and 12 were expressed more highly in SD plants, including *ELF3-2*, a component of circadian clock controlling the flowering regulation (Fu et al., 2009; Figure 1J); while 566 genes in Clusters 13 and 14 were expressed more highly in LD plants.

Clearly, the presence of the *csa* mutation does not substantially affect gene expression in flag leaves that develop under different day lengths, indicating that CSA does not have a prominent regulatory function in leaf tissues. A cluster tree based on the gene expression confirmed that LD and SD samples were generally very well separated, with good pairing between WT and *csa* samples at the same timepoint (Figure 1, A and K and Supplemental Figure S2). An exception was the LD samples at ZT7 and ZT19, which appeared scattered evenly through the tree. A direct comparison of a day and night timepoint (ZT11 and ZT23, respectively) confirmed that few genes were differentially regulated between WT-SD and *csa*-SD, or between WT-LD and *csa*-LD (Supplemental Table S1 and Supplemental Data set S2).

Photoperiod has a weaker effect on endogenous clock genes in anthers than in leaves

A similar comparison between WT anther transcriptomes at two timepoints (day ZT11 and night ZT23) was also performed. An initial comparison between WT-LD and WT-SD anthers revealed that across both timepoints, 182 genes were upregulated and 241 genes were downregulated in the SD anthers (Supplemental Table S2 and Supplemental Data set S3). Closer analysis of eight circadian- or daylength-regulated genes that were differentially expressed in leaves revealed that six of these genes were also differentially expressed in anthers (Supplemental Figure S3). Expression of *CCA1* and *PRR95* in WT anthers differed across SD and LD conditions during both day and night; *RDD1* and *DOF12* exhibited higher expression only at night in LD plants; and *Hd3a* and *HD1* showed differences during the day (Supplemental Figure S3). Clock genes controlled by photoperiodicity in anthers were thus similar to those in leaves, although some of the expression patterns were altered between the two tissues.

Small groups of DEGs may be responsible for male sterility and fertility in *csa* anthers under SD and LD conditions

In *csa* plants, anthers exhibit large developmental defects under SD conditions that lead to male sterility (Zhang et al., 2010); however, under LD conditions, MYB family homologs may function as CSA substitutes, partially restoring fertility (Zhang et al., 2013). We examined gene expression in WT and *csa* anthers in both photoperiods at both timepoints and found 8,211 differentially expressed genes (DEGs) in

total (Supplemental Data set S3). Because expression of CSA was high in daytime and nighttime anthers and corresponded with a large number of common DEGs at both timepoints (Supplemental Data set S1 and Supplemental Table S2), for subsequent analyses we only looked at genes that were differentially expressed in the same way (up or down) at both timepoints for each condition.

By comparing gene expression between *csa* and WT anthers under the SD condition, we found 1,196 genes with decreased, and 151 genes with increased, expression in *csa* anthers that may be the cause of sterility (Figure 2A; Supplemental Table S2 and Supplemental Data set S3). Another comparison between *csa*-LD with *csa*-SD anthers revealed 226 upregulated, and 1 downregulated, genes in the LD anthers, that may be responsible for partial restoration of fertility (Figure 2A; Supplemental Table S2 and Supplemental Data set S3). These 226 genes are the presumptive downstream targets of the CSA homologs substituting for CSA function under LD conditions.

Of these 226 genes upregulated in *csa*-LD anthers, 218 were also among the 1,196 downregulated genes in *csa*-SD compared with WT-SD anthers (Figure 2B), strongly suggesting that these genes may be responsible for the total sterility of *csa*-SD pollen. These 218 genes had a decreasing level of expression, from WT-SD, to *csa*-LD, to *csa*-SD anthers (Figure 2C), suggesting a mechanism that might explain a partial restoration of fertility, but not sufficient to entirely restore WT fertility (Zhang et al., 2013). To better understand this discrepancy in fertility, we examined changes in gene expression between *csa*-LD and WT-LD anthers. A total of 297 genes were downregulated and 495 genes were upregulated, in the transition to full WT fertility (Figure 2A; Supplemental Table S2 and Supplemental Data set S3); of these 495 genes, 299 were also in the 1,196 genes downregulated in *csa*-SD compared with WT-SD anthers. This set of 299 genes likely contains genes responsible for full fertility restoration. A final comparison between WT-SD and WT-LD anthers showed that 241 genes were downregulated and 182 genes upregulated in the SD anthers (Supplemental Table S2 and Supplemental Data set S3); this set of genes is likely responsible for effecting photoperiod response in reproductive development, that is flowering time.

Correlation analysis reveals groups of genes correlated with fertility traits

To understand how these DEGs work together to regulate the male fertility under different photoperiods, weighted gene correlation network analysis (WGCNA) was applied to all 8,211 anther DEGs mentioned above. The DEGs assembled to 11 distinct co-expression modules, each containing 56–1,627 genes, and a gray module containing 10 uncorrelated genes (Supplemental Table S3 and Supplemental Data set S4). An eigengene dendrogram and heatmap was used to identify groups of correlated eigengenes (Supplemental Figure S4, C and D). To understand the biological importance of the modules, we correlated the module eigengenes

(MEs; i.e. the first principal component of a module) of the 11 modules with selected external traits—including sterility, semi-fertility, WT, fertility, *csa*, LD, SD, daytime, and nighttime expression (Figure 3). None of modules showed high correlation with these photoperiod traits (SD or LD expression; Figure 3), confirming our previous findings that transcriptome profiles in the anthers were not strongly affected by daylength variations.

However, several of the modules had strong correlations with fertility traits (Figure 3). MEs of the turquoise module (1,627 genes) and blue module (1,545 genes) were highly correlated with WT-fertility (Figure 3 and Supplemental Table S3). Genes in the turquoise module were most highly expressed in WT-LD anthers and had lowest expression in *csa*-SD anthers (Supplemental Figure S5A), while genes in the blue module had highest expression in the WT-SD anthers (Supplemental Figure S5B). Conversely, MEs in the purple module (115 genes) and red module (609 genes) were most strongly correlated with the male sterile trait (Figure 3; Supplemental Table S3); as such, genes in the red and purple modules were most highly expressed in *csa* anthers (Figure 3; Supplemental Figure S5, C and D). The semi-fertility trait, representing the phenotype of *csa*-LD anthers with partial fertility, correlated most highly with the yellow module; these genes were most highly expressed in *csa*-LD anthers (Figure 3; Supplemental Figure S5E).

Hub genes, which are defined as highly connected genes for co-expression modules (Langfelder and Horvath, 2008), were identified for each module. Four genes were identified as hub genes in the blue module (Table 1). Surprisingly, the expression of these four genes increased in *csa* anthers, especially LOC_Os01g05510 and LOC_Os01g03410, whose expression was not detected in WT rice (Supplemental Data set S1). LOC_Os07g01710 putatively encodes a phytoalkylamine LRR receptor kinase, which is likely to be a receptor of metabolites that change in *csa* plants, especially sugars. LOC_Os11g27370 is a member of UDP-glucosyltransferase domain containing protein family; its increased expression could be due to carbon starvation in the anthers. Two hub genes were identified in the turquoise module, one of which is a putative UDP-glucose 6-dehydrogenase, whose homologs in Arabidopsis are involved in cell wall growth (Siddique et al., 2012).

CSA may direct male fertility through sugar metabolism

The transcriptomic results have provided a set of DEGs responsible for male fertility in response to photoperiod and genotype, and the WGCNA analysis has helped clarify the co-expression patterns of genes responsible for different fertility traits. Our next step was to compare DEGs with genes in selected modules. Venn analysis showed that most of DEGs in the “*csa* sterility” set overlapped with genes in the turquoise (585 genes) and blue (563 genes) modules (Figure 4A). For the 227 “fertility restoration” DEGs, 184 of them were overlapped with turquoise module and 35 genes

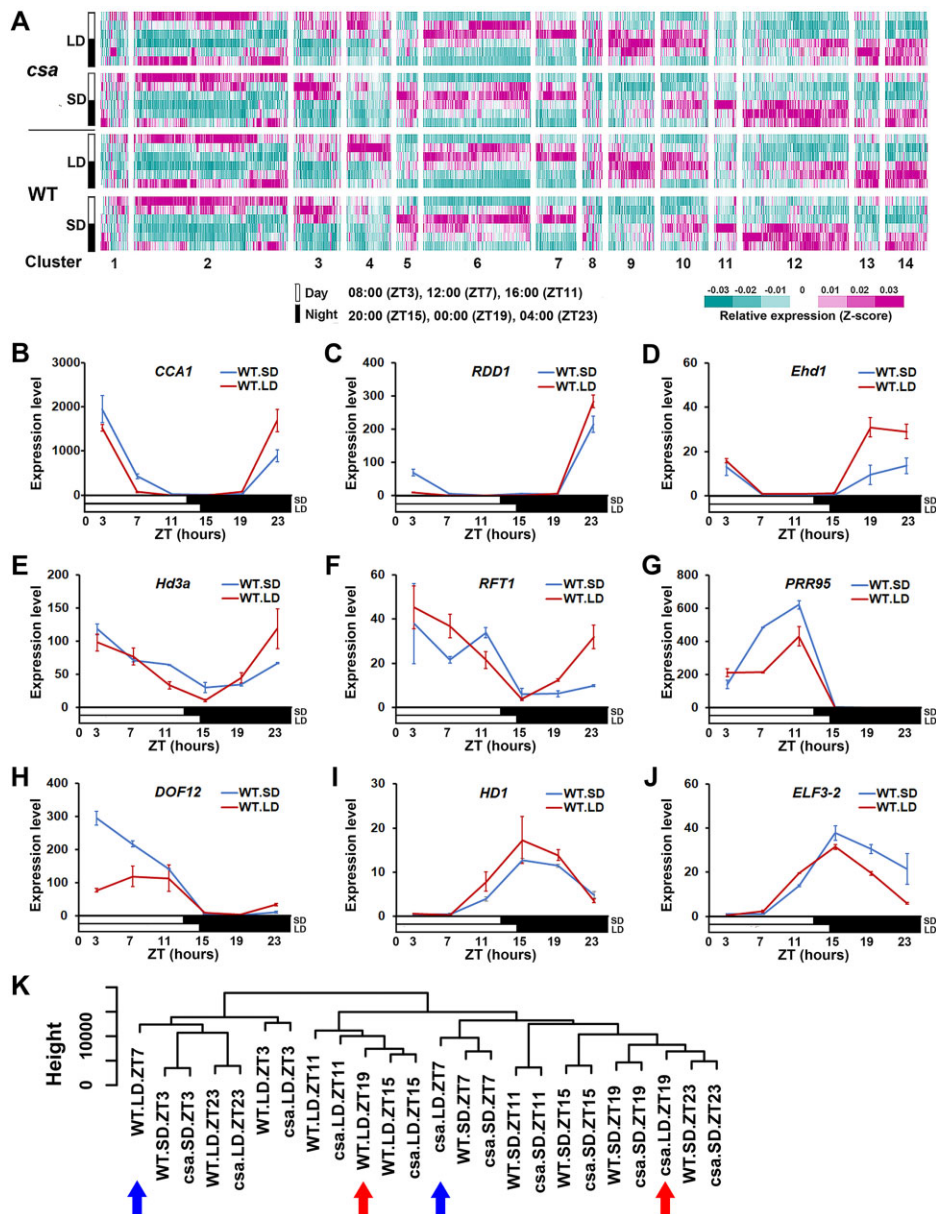


Figure 1 Transcriptome variations in WT and *csa* leaves under LD and SD conditions. A, 6,266 transcripts with different expression patterns due to genotype or photoperiod assemble into 14 clusters across 6 timepoints. White bars indicate day timepoints (ZT3, ZT7, and ZT11), while black bars indicate night timepoints (ZT15, ZT19, and ZT23). B–J, Expression pattern of genes involved in circadian rhythm regulation and photoperiod sensing in WT leaves. Expression level indicates mean \pm STD of RPKM from RNA-seq data, $n = 2$. K, Sample clustering of the transcriptomes in leaves under different conditions. Note the differences between WT and *csa* leaves under LD conditions at ZT7 (12:00) and ZT19 (00:00; Arrows highlight the differences at ZT7 and ZT19). STD, standard deviation.

were found in the blue module (Figure 4B). Finally, a number of DEGs in the “WT fertility” set overlapped with genes in the yellow WGCNA module, which has high correlation with the semi-fertility trait, indicating that these overlapped genes play important roles in fertility restoration under LD conditions (Figures 3 and 4C). Genes present in both DEG sets and modules known to correlate with fertility are likely to participate in the anther development.

To make clear the regulatory function of CSA and its replacement during LD anther development, we applied gene ontology (GO) analysis to genes in the selected DEG sets

and WGCNA modules (Table 2; Supplemental Table S4). For the 1,196 downregulated genes in the “*csa* sterility” DEG set (yellow region; Figure 2A), GO enrichment revealed that six GO terms are significantly over-represented, including cell wall modification, pollen tube growth, actin filament depolymerization, carbohydrate metabolic process, amino acid transmembrane transport, and transmembrane transport. Five of the six GO terms were the same as that of turquoise module (Table 2; Supplemental Table S4), confirming that the downregulated genes among these GO terms play important roles in male fertility. Among these six GO terms,

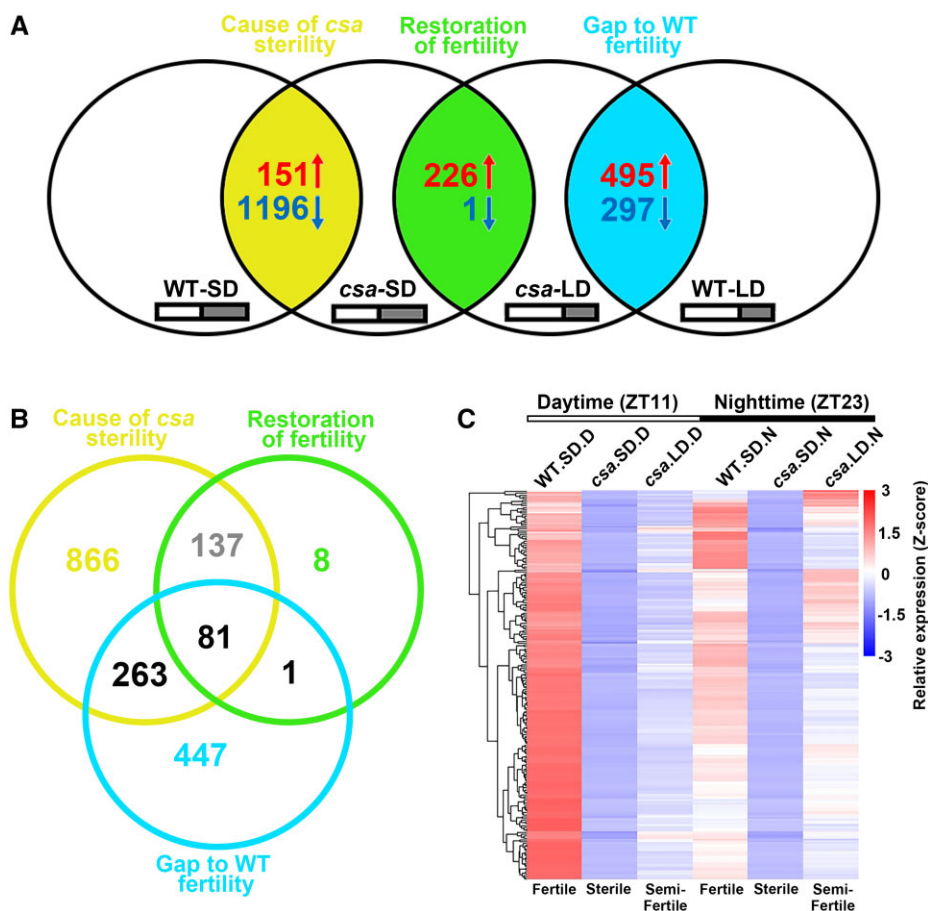


Figure 2 DEGs in WT and *csa* anthers that may drive male sterility and fertility in response to photoperiod. A, DEGs between different anther samples that may be responsible for driving fertility differences in pollen. Yellow region, DEGs in *csa*-SD compared with WT-SD that may cause pollen sterility in *csa*-SD anthers; green region, DEGs in *csa*-LD compared with *csa*-SD, whose changes in expression may drive partial restoration of fertility in *csa*-LD pollen; blue region, DEGs in WT-LD compared with *csa*-LD, whose expression may be responsible for full restoration of fertility. Red arrows, upregulated; blue arrows, downregulated. B, Overlap of DEGs expressed in more than one tissue; however, the direction of up or downregulation may not be conserved in the overlap. C, Expression of 218 overlapped genes among the WT-SD, *csa*-SD, and *csa*-LD.

genes involved in carbohydrate metabolic and transmembrane transport had the most enrichment, with 42 genes and 44 genes, respectively. Downregulated genes in carbohydrate metabolism encoded enzymes involved in both sucrose and hexose (glucose, fructose, mannose, and galactose) metabolism, including CWINs, SWEETs, and MSTs (Table 3). Two invertase family members, *INV4* and *CWIN6*, were observed to have decreased expression in the *csa* compared with WT on SD, with \log_2 fold change (FC) of -3.06 and -20 , respectively (Table 3). The two genes are important components of the sucrose phloem transport pathway, thus decrease of their expression indicated the variation of the sink strength for carbohydrate partitioning. Meanwhile, 7 SWEET family genes and 14 MSTs were also less highly expressed in the “*csa* sterility” DEG set (Table 3), strongly suggesting that the *csa* male sterile phenotype may be due to defects in sugar partitioning, particularly for glucose and galactose. Altered glycometabolism could also explain changes in expression of genes encoding cell wall modification, which relies on sugar substrates (Lee et al., 2007) and actin filament depolymerization, which participates in cell

wall development (Supplemental Table S5; Geitmann et al., 1996; Chen et al., 2007b).

GO analysis of the “fertility restoration” DEG set also highlighted biological processes related to cell wall organization, carbohydrate metabolic, and actin filament organization (Table 2), including *INV4*, *SWEET14*, and several MST genes (i.e. *AZT3*, *STP6*, and *AZT5*; Table 3). Meanwhile, 19 genes involved in cell wall development and 4 actin filament organization genes were also increased in this DEG set (Supplemental Table S6). Increased expression of these genes in the “fertility restoration” DEG set suggests that sugar metabolism and cell wall development were partially recovered in *csa*-LD anthers.

CSA downstream target genes are involved in sugar partitioning

The expression patterns of several key genes known to be involved in sugar partitioning were verified by reverse transcription quantitative PCR (RT-qPCR). We examined two genes encoding invertases (*CWIN6* and *INV4*), three genes encoding SWEET sugar transporters (*SWEET5*, *SWEET6a*, and

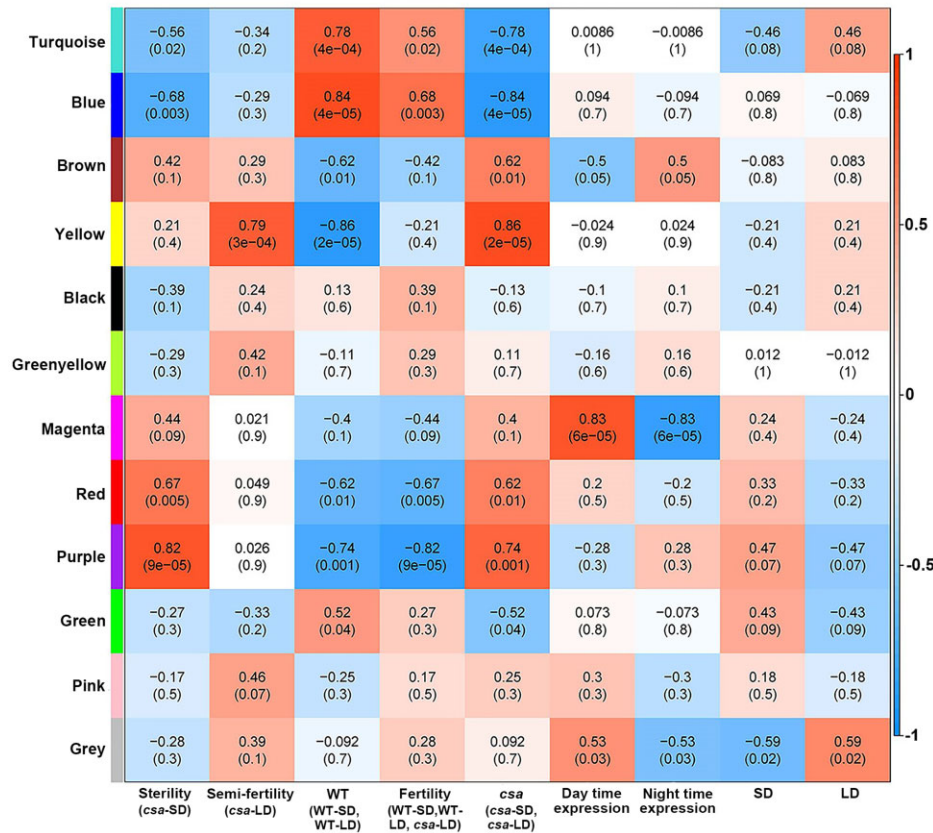


Figure 3 Relationships of modules and traits. Heatmap of the correlation between MEs and traits. Each row in the heatmap corresponds to a consensus module and each column to a fertility or photoperiod trait. Numbers in the heatmap report the correlations of MEs and traits, with the *P*-values given in brackets. A deeper color corresponds to a higher correlation coefficient.

Table 1 Identities of hub genes in selected co-expression modules

Modules	Numbers	Hub Genes	Gene annotation
Turquoise	1,627	LOC_Os12g25690	UDP-glucose 6-dehydrogenase
Blue	1,545	LOC_Os04g35580	Unknown function
		LOC_Os01g05510	Unknown function
		LOC_Os01g03410	Ubiquitin ligase
		LOC_Os11g27370	UDP-glucosyltransferase domain containing protein
		LOC_Os07g01710	Phytosulfokine LRR receptor kinase

SWEET6b) and three genes encoding MSTs (*MST1*, *STP14*, and *STP18*), all of which were highly expressed in sink tissues, such as roots and anthers (Figure 5A). Expression of all of these genes was significantly downregulated in *csa*-SD anthers compared with WT-SD anthers; in *csa*-LD anthers, six genes were also downregulated compared with WT anthers, while expression of *CWIN6* and *SWEET6b* appeared to be close to that in WT-SD anthers (Figure 5B). RT-qPCR confirmed the drop in expression levels of these eight genes in *csa*-SD anthers, but expression of all eight genes was higher in *csa*-LD anthers compared with *csa*-SD anthers, and in the cases of the five invertase and *SWEET* genes, approached WT-LD expression levels (Figure 5, C–J).

Sequence analysis of the 2-kb upstream promoter regions of these eight genes revealed potential MYB transcription factor binding sites in all of them (Figure 6A); the promoter for *MST8*, known to bind CSA, was used as a positive control

(Zhang et al., 2010). Transgenic rice plants expressing a full-length FLAG-tagged CSA fusion protein were used in chromatin immunoprecipitation (ChIP) assays to determine whether CSA directly binds to the promoters of candidate genes. The ChIP-qPCR assays revealed at least two CSA binding sites in the promoters of all eight genes (Figure 6, B–I), similar to results observed in the *MST8* positive control (Figure 6J).

Dual-luciferase (LUC) assays were performed in *Nicotiana benthamiana* leaves to verify the CSA protein activation of these genes. CSA was transiently co-expressed with a LUC reporter under control of each of the eight genes individually (Figure 6K), revealing that expression of these eight genes was promoted by CSA in *N. benthamiana* leaves (Figure 6L).

Subsequently, we constructed a loss-of-function double *cwin6 inv4* mutant, a triple *sweet5 sweet6a sweet6b* mutant, and a triple *mst1 stp14 stp18* mutant using CRISPR/Cas9

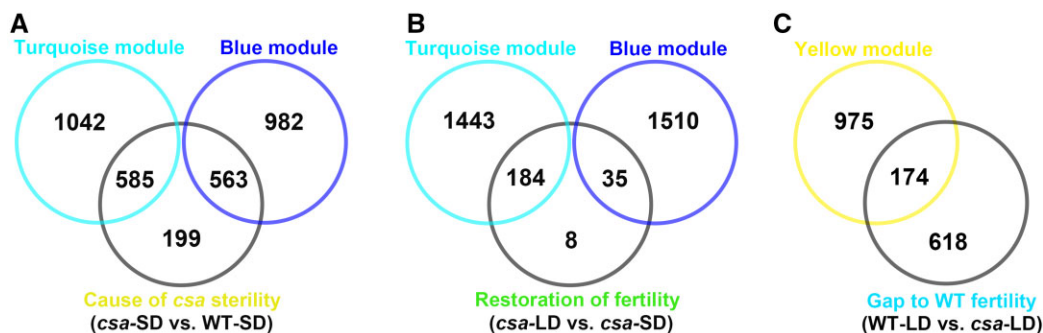


Figure 4 Overlapping of DEGs and MEs in the selected modules. A, Venn analysis of MEs in turquoise module, MEs in blue module, and DEGs in *csa*-SD compared with the WT-SD anthers (sterility DEGs). B, Venn analysis of MEs in turquoise module, MEs in blue module, and DEGs in *csa*-LD compared with the *csa*-SD (restoration of fertility DEGs). C, Venn analysis of MEs in yellow module and DEGs in *csa*-LD compared with WT-LD (gap to WT fertility DEGs).

Table 2 Biological process analysis by GO of the “*csa* sterility” DEG set and the “fertility restoration” DEG set

GO term	Description	Gene	P-value	FDR
Downregulated genes of the “ <i>csa</i> sterility” DEG set (<i>csa</i> -SD versus WT-SD)				
GO:0009827	Plant-type cell wall modification	19	2.35E-09	2.29E-06
GO:0009860	Pollen tube growth	22	6.07E-08	2.95E-05
GO:0030042	Actin filament depolymerization	7	9.87E-08	3.20E-05
GO:0005975	Carbohydrate metabolic process	42	1.44E-07	3.50E-05
GO:0003333	Amino acid transmembrane transport	11	1.12E-04	2.18E-02
GO:0055085	Transmembrane transport	44	3.15E-04	5.10E-02
Upregulated genes of the “fertility restoration” DEG set (<i>csa</i> -LD versus <i>csa</i> -SD)				
GO:0043086	Negative regulation of catalytic activity	11	2.04E-09	6.29E-07
GO:0009831	Plant-type cell wall modification	6	4.49E-07	6.92E-05
GO:0019953	Sexual reproduction	5	1.52E-06	1.37E-04
GO:0009828	Plant-type cell wall loosening	6	1.77E-06	1.37E-04
GO:0071555	Cell wall organization	14	1.38E-05	8.49E-04
GO:0005975	Carbohydrate metabolic process	13	8.01E-05	4.11E-03
GO:0009827	Plant-type cell wall modification	6	1.06E-04	4.41E-03
GO:0042989	Sequestering of actin monomers	2	1.15E-04	4.41E-03
GO:0009860	Pollen tube growth	7	2.02E-04	6.91E-03
GO:0007015	Actin filament organization	4	3.81E-04	1.17E-02
GO:0009826	Unidimensional cell growth	6	1.55E-03	4.34E-02

mutagenesis (Figure 7, A–C). All three mutants exhibited normal vegetative growth. Pollen staining revealed that *cwin6 inv4* and *sweet5 sweet6a sweet6b* pollen are partially fertile (69% and 72% fertile, respectively; Figure 7, D and E). The *mst1 stp14 stp18* pollen was 88% fertile, close to WT levels (Figure 7, D and E). As all of these genes are involved in sugar metabolism, we measured sugar contents in the flag leaf, palea/lemma, and anther in the mutants under SD conditions (Figure 7, F–H); during normal development, sugars usually flow from the flag leaf source tissues via the palea/lemma to the anther sink tissues. The *cwin6 inv4* revealed significantly less glucose and fructose but more sucrose in the anthers compared with WT, suggesting that loss of function of the two invertases compromised the decomposition from sucrose to monosaccharides, resulting in lower levels of starch accumulation (Figure 7H and Supplemental Table S7). Much higher levels of monosaccharides (glucose and fructose) accumulated in the palea and lemma in the SWEET and MST triple mutants compared with WT (Figure 7G and Supplemental Table S7), which may have reduced sucrose inflow, causing sucrose to

accumulate in flag leaves (Figure 7F and Supplemental Table S7), and reduced monosaccharide transport into anthers (Figure 7H and Supplemental Table S7), further reducing levels of starch accumulation from flag leaves. These results indicated that these mutants (double *cwin6 inv4* mutant, triple *sweet5 sweet6a sweet6b* mutant, and triple *mst1 stp14 stp18* mutant) showed similar accumulation of sucrose in the flag leaves and decreased monosaccharides (glucose and fructose) and starch in the anther to the *csa* mutant. Thus, the overall partitioning of sugars from source to sink tissues was impaired when key transporters were not functional.

Other roles for CSA in plant development

While CSA clearly plays a role in directing sugar metabolism in anthers, it may also have other regulatory effects on plant growth and development. Although the *csa* mutation had little effect in leaf tissues, nine downregulated and seven upregulated genes were found in *csa* leaves (Supplemental Table S1 and Supplemental Data set S2). Of these, eight were also altered in the *csa*-SD versus WT-SD anther samples (the “*csa* sterility” DEG set in Supplemental Table S2 and

Table 3 DEGs involved in sugar metabolism in the four different DEG sets

“ <i>csa</i> sterility” DEG set	“fertility restoration” DEG set	“WT fertility” DEG set	“photoperiod-response” DEG set
CWIN6	INV4	INV2	INV1
INV3	SWEET14	INV4	INV3
INV4	SWEET1B	NIN7	NIN7
SWEET14	AZT3	OsSUT3	SWEET11
SWEET15	STP6	SWEET11	SWEET14
SWEET1B	AZT5	SWEET13	SWEET2A
SWEET2A	–	SWEET14	SWEET2B
SWEET5	–	SWEET15	SWEET6A
SWEET6A	–	SWEET1A	SWEET6B
SWEET6B	–	SWEET4	STP8
STP8	–	SWEET5	STP7
AZT1	–	SWEET6A	STP4
AZT3	–	SWEET6b	STP14
PLT1	–	STP7	STP1
STP4	–	AZT3	STP18
ERD3	–	STP1	STP3
STP2	–	STP18	STP6
MST1	–	INT3	PLT5
STP16	–	STP6	STP5
STP18	–	STP5	AZT5
INT3	–	STP27	PLT12
PLT4	–	AZT5	PLT13
STP14	–	PLT12	PLT14
STP3	–	PLT13	–
STP21	–	PLT14	–
STP22	–	–	–
STP6	–	–	–
PLT5	–	–	–
PLT3	–	–	–
AZT5	–	–	–
PLT13	–	–	–
PLT14	–	–	–
PLT15	–	–	–

Supplemental Data set S3), indicating that CSA has some common functions in the anther and leaf (Supplemental Table S8). These genes encode a brix domain containing protein (LOC_Os01g05530), a protein involved in vacuolar import and degradation (LOC_Os01g05090), an arginyl-tRNA synthetase (LOC_Os01g06510), a core histone domain containing protein (LOC_Os01g05610), a kinesin heavy chain protein (LOC_Os01g01570), and three proteins of unknown function (LOC_Os01g05510, LOC_Os03g45220, and LOC_Os01g05289). These genes presumably direct or affect source and sink cooperation, especially LOC_Os01g05510, which is also one hub gene of blue module (Table 1).

Discussion

Photoperiod changes reveal feedback processes of endogenous oscillators in WT leaves

PGMS lines, whose fertility is dependent on photoperiod, are an essential tool for hybrid rice breeding (Yuan, 1994), but the mechanisms by which photoperiods are sensed and translated to male reproductive development are not yet understood. Transcriptome profiling of Nongken 58S, the most widely used PGMS line, suggests general downregulation of genes under LD conditions (Wang et al., 2011), but because source leaf was not included in the analysis, the process of receiving and transmitting daylength signals could

not be studied. Photoreceptors, such as phytochromes and cryptochromes, play an essential role in light signal reception (Song et al., 2010). In this study, we observed marked difference in transcriptome profiling of WT leaves under different photoperiods (Figure 1A). However, genes encoding light receptors, such as *PHYA*, *PHYB*, *PHYC*, *CRY1A*, and *CRY1B*, did not reveal significant transcriptional variation under different photoperiods (Supplemental Data set S1), which suggests that their expression levels may not influence the photoperiod response directly. However, we have found that expression of several circadian clock components, specifically *CCA1* and *PRR95*, varied in WT leaves under SD and LD conditions. It has been reported that photoperiod changes altered the phases of core clock genes with 1–4 h peak time differences among different photoperiods in Arabidopsis (Flis et al., 2016). For example, the peak of *AtCCA1* transcripts delayed for about 2.7 h in 18-h photoperiod compared with 6-h photoperiod, and the phase shifting varied as the photoperiod changes (Flis et al., 2016). Interestingly, their results also showed 0.4 h earlier peak of *AtLHY* transcripts in 18-h photoperiod than that in 12-h photoperiod (Flis et al., 2016), consistent with our data of *CCA1* expression showing the earlier peak time under LD condition (14 h) than that of SD condition (12 h) (Figure 1B). We also observed that *PRR95* transcripts have lower amplitude under

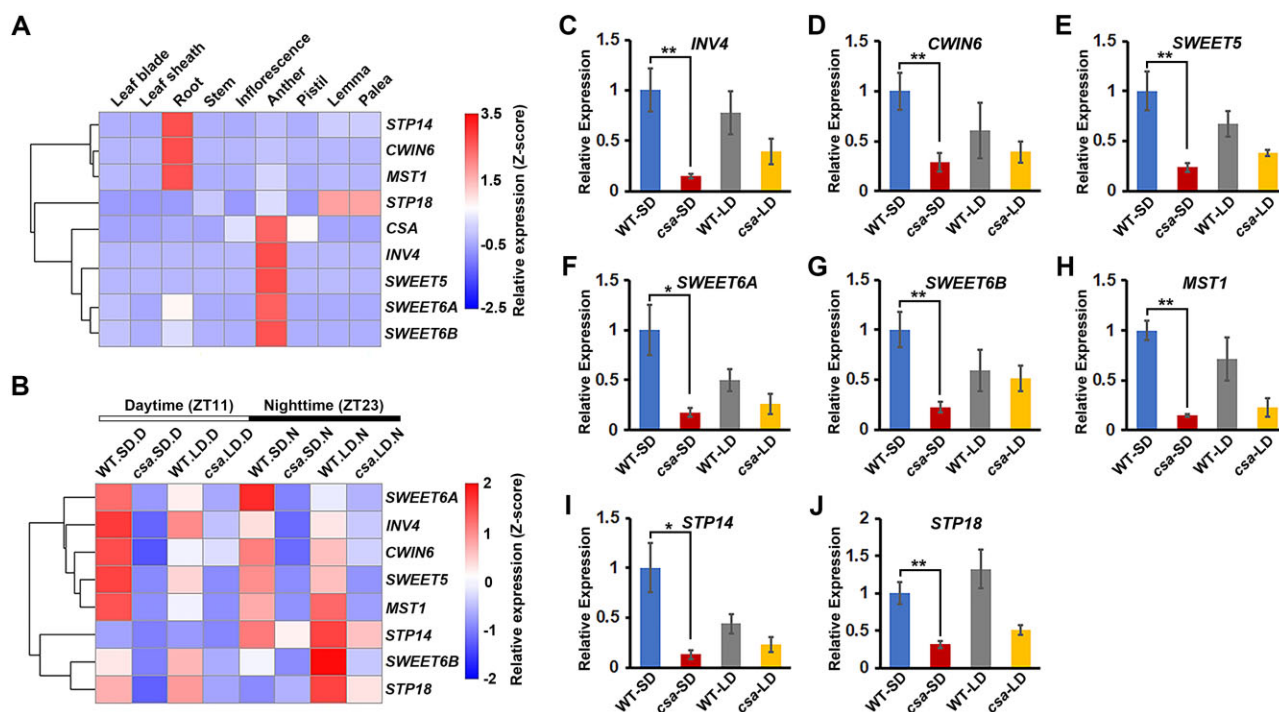


Figure 5 Expression of candidate target genes downstream of CSA. A, Spatiotemporal expression profiles of candidate CSA target genes (expression data from RiceXPro database, <https://ricexpro.dna.affrc.go.jp/>). B, Expression of candidate genes in the *csa* and WT anthers under SD and LD conditions (RNA-seq data). C–J, Verification of the expression patterns of the candidate genes by RT-qPCR in *csa* and WT anthers. Data indicate mean \pm STD of three biological replicates; * $P < 0.05$, ** $P < 0.01$ (Student's *t* test).

LD condition than SD condition (Figure 1G), which is consistent with the variation of *AtPRR5* in Arabidopsis (Flis et al., 2016). These results suggested that these may be components responsible for responding to changes in light signals, and transmitting these changing signals to downstream pathways.

Signals of photoperiod change are transduced from leaves to anthers

Anthers are sequestered within leaf sheaths and cannot directly respond to environmental cues, especially light. In Arabidopsis, *FT* transcription to signal onset of flowering is activated in the vascular tissues of leaves, and transported to the shoot apical meristem to induce flowering (Liu et al., 2013). In this study, a relatively large number of DEGs was observed between WT-LD and WT-SD anthers, indicating the transduction of photoperiod cues from leaves to anthers (Supplemental Table S2). In WT anthers, we observed similar expression patterns of *CCA1* and *PRR95* with leaves (Figure 1 and Supplemental Figure S3), which suggests that changes in circadian rhythm were transduced from leaves to the anthers. These results are consistent with our recently reported transcriptome profiles of rice anther, which observed similar changes of *CCA1* and *PRR95* expression in SD and LD anthers (Sun et al., 2021b). Other clock-related genes differentially expressed in the leaves did not exhibit significant changes in anther expression (e.g. *RFT1*), indicating that the switch to photoperiod-sensitive regulation of male

development may be governed by a subset of circadian clock genes.

In Arabidopsis, expression of *CO*, the vital flowering control gene, is governed mainly by the circadian clock, while light signaling regulates *CO* protein activity (Suárez-López et al., 2001; Song et al., 2012). *HD1*, the rice *CO* homolog, is also an important regulator of flowering control that activates expression of the florigen gene, *HD3a*. Consistent with a previous report that *Hd1* promotes *HD3a* expression under SD and represses it under LD conditions (Sun et al., 2014), here we observed that *HD1* expression is high and *Hd3a* expression is low in LD anthers (Supplemental Figure S3). Differential expression of *HD1* is co-regulated by the circadian clock and light signals; for example, *HD1* expression in anthers is elevated under LD conditions compared with SD conditions, following reduced expression of *PRR95* (Supplemental Figure S3), implying that expression of *HD1* may be related to the core clock gene *PRR95*.

Lack of functional CSA leads to disrupted diurnal clock gene expression in anthers

CSA had extremely low expression in the leaves and very high expression in the anthers (Supplemental Data set S1). When comparing the transcriptomes of *csa*-SD and WT-SD anthers, numerous rhythmic genes including *CCA1*, *TOC1*, *PRR37*, *PRR73*, *PRR95*, *PRR59*, *GI*, and *ELF3* revealed significantly differential expression during the day and/or night (Supplemental Figure S6), indicating that the absence of *CSA* regulatory function can greatly influence oscillators of

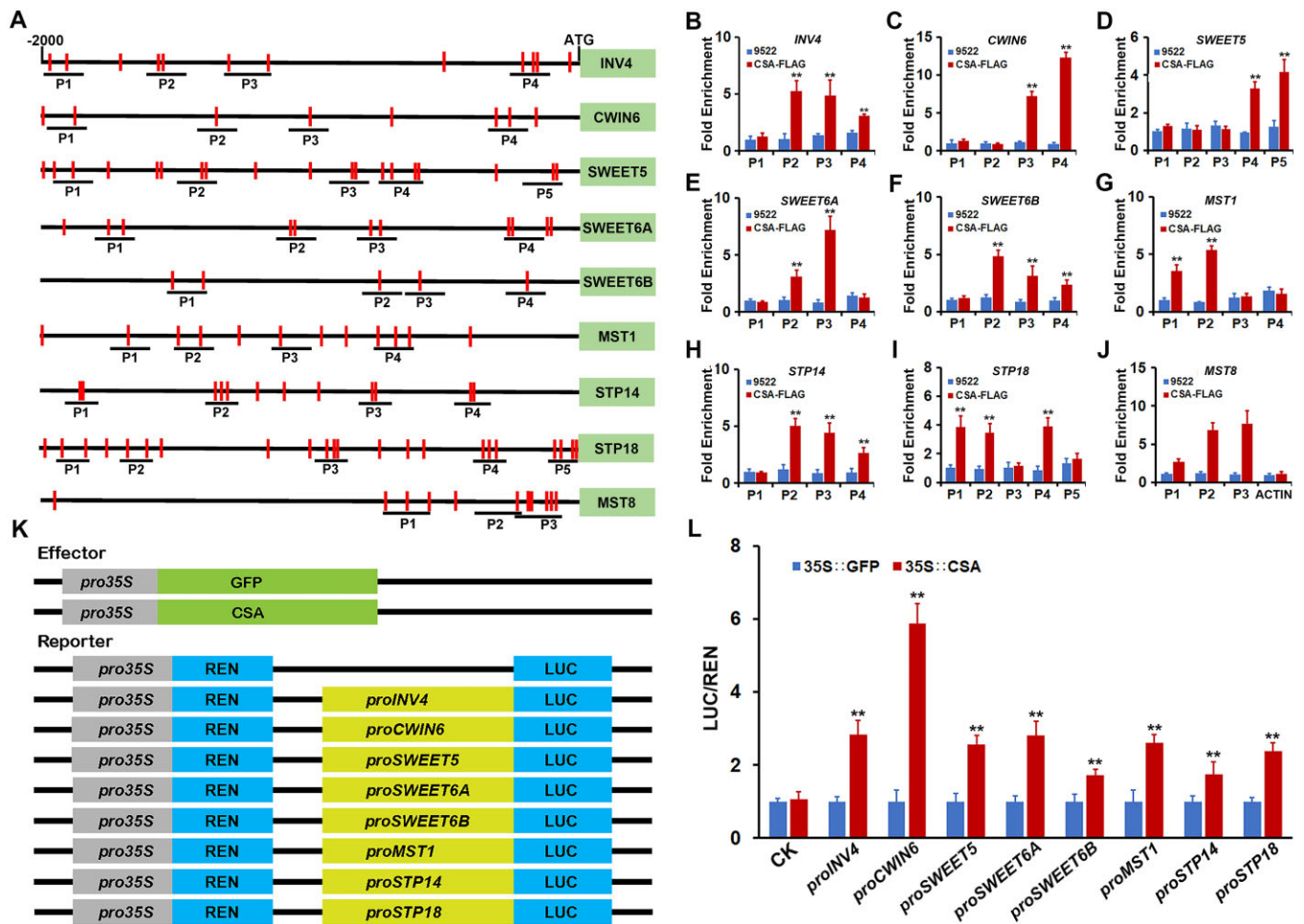


Figure 6 Verification of direct target genes of CSA. A, Predicted CSA binding sites (MYB sequences) in the promoters of candidate CSA target genes. Red vertical lines indicate MYB binding sites. B–J, ChIP-qPCR analysis revealed direct association of CSA with promoter elements for all genes. Data indicate mean \pm STD of three biological replicates; $**P < 0.01$ (Student's *t* test). K, Effector and reporter constructs for dual-LUC assays. The CSA gene was under control of the 35S promoter. Negative controls were the GFP effector construct and the reporter plasmid with no promoter (CK). L, Relative LUC activity for each reporter/effector construct pair reveals direct interaction of CSA proteins and the promoters of the candidate genes. Data indicate the ratio of LUC/REN from five biological duplications (mean \pm STD); $**P < 0.01$ (Student's *t* test).

the circadian system. Expression of many genes linking oscillator and photoperiod signals did not present difference in the *csa* leaves (Supplemental Data set S1), indicating that CSA may act as an important factor modulating a possible peripheral clock, specifically in anthers. Consistently, we previously reported that 5,852 co-expressed genes significantly correlate with photoperiod changes in the bioinformatic analysis of anther transcriptome profiles, and CSA is a key factor of these genes, which may play important roles in photoperiod response (Sun et al., 2021b). Higher transcription of CSA was observed under LD compared with SD conditions, consistent with a previous report (Zhang et al., 2013); this higher expression is likely to be regulated by photoperiod signal transduction from leaf to anther.

Regulatory network of CSA on the anther development

Our results showed that CSA performs important regulatory functions mainly in anthers via a considerable number of

DEGs (Figure 2 and Supplemental Table S2). Through co-expression analyses, two sets of genes were found to direct WT fertility in response to CSA, that is the turquoise and blue modules, which have large portions of overlap with the “*csa* sterility” DEG set (Figures 3 and 4A). LOC_Os12g25690, a UDP-glucose dehydrogenase (UGDH) protein, was one of the hub genes in the turquoise module (Table 1). UGDH plays a key role in the nucleotide sugar biosynthetic pathway, producing UDP-glucuronic acid as a common precursor for the cell wall monosaccharide components, that is arabinose, xylose, galacturonic acid, and apiose (Reboul et al., 2011). Four hub genes in the blue module included LOC_Os11g27370, which encodes a UDP-glucosyl transferase protein likely to be an important component of the sugar metabolism or cell wall formation; and LOC_Os01g05510, which although of unknown function, is downregulated in both flag leaves and anthers of *csa* plants under SD condition. The roles of these hub genes are similar with the predicted function of the “*csa* sterility” DEG set by

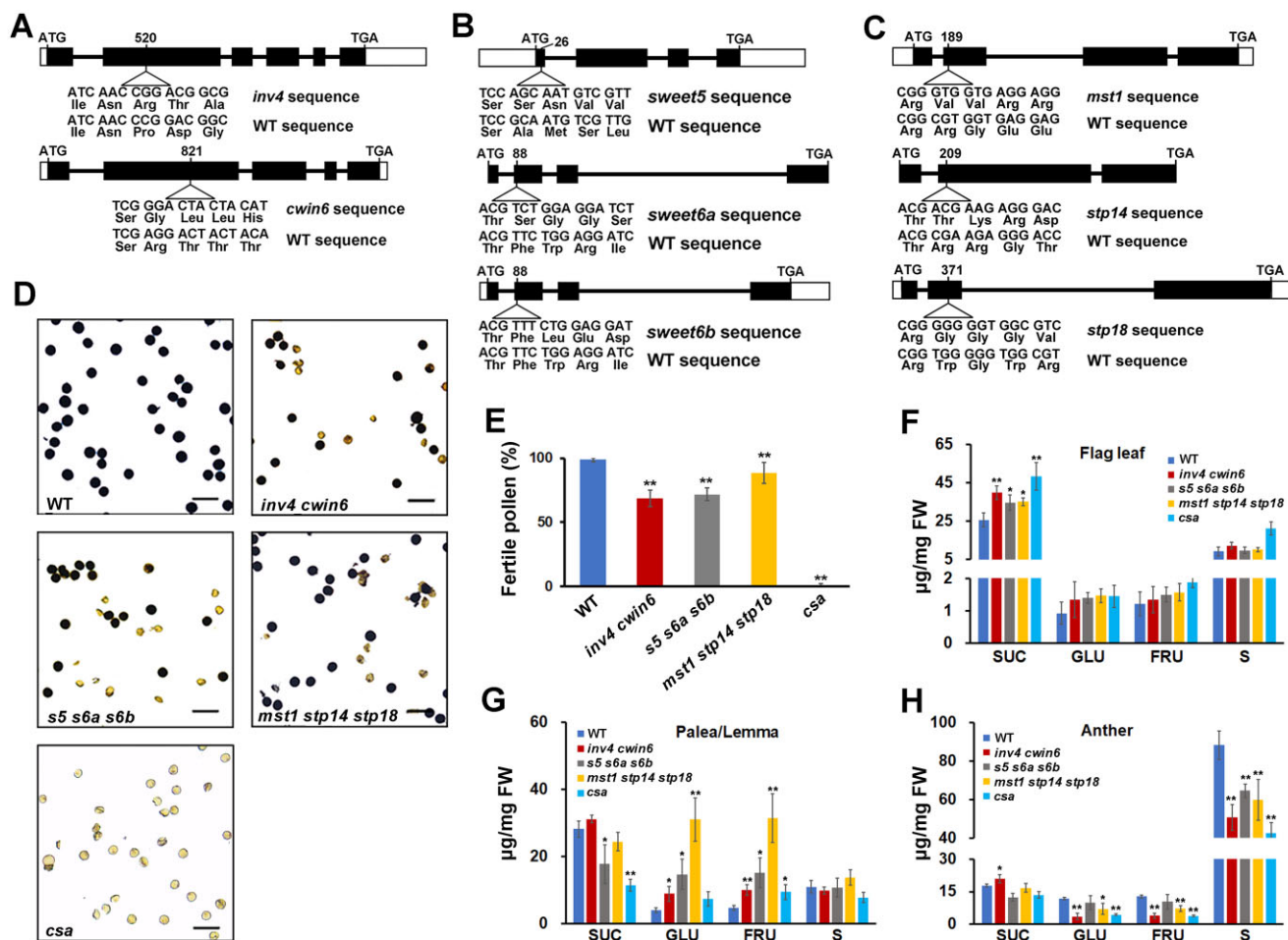


Figure 7 Phenotyping mutants of CSA target genes. A, Mutation sites in *INV4* and *CWIN6* genomic sequences. B, Mutation sites in *SWEET5*, *SWEET6a*, and *SWEET6b* genomic sequences. C, Mutation sites in *MST1*, *STP14*, and *STP18* genomic sequences. D, Iodine staining of pollen grains from WT and mutant anthers. Viable pollen grains stain darkly. Scale bar, 100 µm. E, Percentage of fertile pollen grains in WT and mutant anthers. Data indicate mean ± STD of three pollen grains from each of three plants. Significant differences were assessed using Student's *t* test compared with WT (***P* < 0.01). F–H, Soluble sugar and starch content in flag leaf (F), palea/lemma (G), and anthers (H) of WT and mutant plants. Data indicate mean ± STD of three biological replicates. Significant differences were assessed using Student's *t* test compared with WT (**P* < 0.05, ***P* < 0.01). *s5 s6a s6b*, *sweet5 sweet6a sweet6b*; SUC, sucrose; GLU, glucose; FRU, fructose; S, starch.

GO analysis, supporting the role of CSA in regulating cell wall and sugar metabolism (Table 2).

CSA regulates the sink strength in sugar partitioning

As a sink tissue, the anther requires carbohydrate supply from source tissues for pollen development and maturation (Zhang and Wilson, 2009). In plants, various sugar transporters including invertases, SWEETs, and MSTs, are engaged in the transport of sugars from source to sink organs via the phloem (Ruan, 2014). In this study, we found carbohydrate metabolism is the core process regulated by CSA for the anther development. By comparing *csa*-SD and WT-SD transcriptomes, we found expression changes in 3 *INV*, 7 *SWEET*, and 23 *MST* genes (Table 3), and found 8 genes that are regulated by CSA directly: 2 genes encoding invertases (*CWIN6* and *INV4*); 3 genes encoding SWEETs (*SWEET5*, *SWEET6A*, and *SWEET6B*); and 3 genes encoding MSTs (*MST1*, *STP14*,

and *STP18*) (Figures 5 and 6). In the semi-sterile *cwin6 inv4* mutant, hydrolysis of sucrose to glucose and fructose is blocked in the anther, resulted in an insufficient supply of monosaccharides during the anther development (Figure 7, D and H). The triple *sweet5 sweet6a sweet6b* mutant was also partially sterile (Figure 7D). *SWEET5* has been reported to function as a galactose transporter (Zhou et al., 2014); this hexose sugar is a key component of the plant cell wall. These three SWEETs may work redundantly as transporters of galactose, whose function is compromised in the absence of CSA regulation. The triple *mst1 stp14 stp18* mutant accumulated glucose and fructose in the palea and lemma (Figure 7G), which suggests that these proteins function in monosaccharide transport from palea and lemma to the anther. In the absence of CSA, the functions of these sugar transport proteins were affected, resulting in *csa*-induced male sterility.

Source activity and sink strength are two important factors to influence the sugar transport efficiency (Bihmidine

et al., 2013), which can greatly affect agricultural crop yields. CSA plays important roles in regulating the sink strength by controlling numerous CWIN, SWEET, and MST proteins. As none of genes encoding proteins involved in sugar transport were observed in the *csa* leaves (Supplemental Data set S1), the CSA regulatory function must occur in the sink tissues.

CSA controls cell wall synthesis in anther development

The cell walls of *csa*-SD anthers are abnormal, being whiter and smaller than those of the WT anther (Zhang et al., 2010). In this study, we have found multiple galactose metabolism genes are downregulated in *csa*-SD compared with WT-SD anthers (Table 2), which would have downstream effects on cell wall growth. Pectins, in particular, are galactose-rich polysaccharides that help to lock microfibrils of the cell walls and determine the wall porosity and wall thickness (Cosgrove, 2005), and defects in their biosynthesis may explain the abnormal *csa* anther phenotype.

In addition, actin filament depolymerization was also affected in the *csa*-sterility DEG set (Table 2). Downregulation of key genes involved in this process, such as LOC_Os07g20170, LOC_Os07g30090, LOC_Os10g37670, LOC_Os04g51440, LOC_Os01g03510, LOC_Os02g44470 and LOC_Os04g46910 (Supplemental Data set S3), can affect biosynthesis of myosins, which direct maintenance of cell shape and vesicle transport (Vale, 2003). One rice myosin, myoXIB, has been shown to control pollen development by photoperiod-sensitive protein localization (Jiang et al., 2007).

CSA-regulated processes can be induced by other pathways to partially restore fertility under LD conditions

In previous research, we speculated that several homologs of CSA may be responsible for regulating anther development under LD conditions (Zhang et al., 2013). A more recent report confirms that CSA2, a homolog of CSA, plays a critical role in male fertility under LD conditions, and *csa2* exhibits semi-sterility due to defects in sugar transport and aborted pollen maturation (Wang et al., 2021). In this study, we found that some sugar and cell wall metabolic processes, compromised in *csa*-SD anthers, were restored in *csa*-LD anthers. Expression of these 218 genes, likely induced by CSA homologs or other MYB transcription factors, was higher in *csa*-LD than *csa*-SD anthers, but still not quite as high as in WT anthers (Figure 2, B and C). These results are consistent with the report of CSA2 function, with common downstream regulatory targets, and provide a good explanation for *csa2* mutant semi-sterility (Wang et al., 2021). Activation of fertility pathways by CSA2 under LD conditions was not completely effective, resulting in only partial restoration of male fertility.

In summary, leaves are the main tissues that respond to photoperiod changes, and transduce photoperiod signals to sink tissues, including anthers, via components of the core clock. Under SD conditions, CSA influences anther

development by controlling a series of genes directly or indirectly involved in sugar partitioning and cell wall development. Under LD conditions, CSA homologs, rather than CSA itself, promote similar downstream genes to regulate anther development. Further study on the roles and redundancies between CSA and its homologs, and their common downstream targets, have important implications for uncovering the mechanisms of PGMS and the development of the two-line hybrid rice.

Materials and methods

Plant growth conditions

WT and *csa* mutant rice (*O. sativa* ssp. *japonica*) were grown in paddy fields around Shanghai. Seeds were sown by early May and transplanted into hydroponics box containing 0.5 × Murashige and Skoog medium (PhytoTechnology Laboratories, Lenexa, KS, USA) and grown in controlled environment chambers (30°C/22°C [day/night], 70% relative humidity, and 15-h light/9-h dark photoperiod). Seedlings were transplanted into paddy fields by the end of May. By the middle of August (initiation of reproductive development), the daylength is ~14 h (LD photoperiod (August 1, 04:40–19:20; August 15, 04:55–19:05). Rice plots (WT and *csa*) were divided into two groups and SD photoperiod (12-h light) was simulated by covering plants in one group with lightproof plastic film at about 16:55. The CRISPR/Cas9 mutants described below were grown under SD field conditions.

Tissue collection, RNA extraction, and sequencing

Leaves and anthers were collected at Stages12 of anther development (Zhang and Wilson, 2009). About 3 cm of flag leaves were sampled every 4 h over 1 day for both photoperiods at ZT3 (08:00), ZT7 (12:00), ZT11 (16:00), ZT15 (20:00), ZT19 (00:00), and ZT23 (04:00), and ~100 mg anthers from the same tiller were harvested at ZT11 (16:00) and ZT23 (04:00) timepoints (Supplemental Figure S1). Two biological repeats were harvested for each sample, frozen immediately in liquid nitrogen, and stored at –80°C.

Total RNA, excluding miRNAs, was extracted using TRIzol (Life Technologies, Carlsbad, CA, USA) for RNA sequencing according to the manufacturer's protocol. cDNA libraries were prepared with the FastQuant RT Kit with DNase (Tiangen, Beijing, China), according to manufacturer's instructions. cDNA libraries were sequenced with Ion Proton platform (Life Technologies, Carlsbad, CA, USA) by Novusbio Ltd (Shanghai, China). The raw sequence data were inspected by FastQC (version 0.11.1) and mapped to the rice reference genome with the RGAP version 7 database from the MSU Rice Genome Annotation Project using MapSplice version 2.1.8 (Wang et al., 2010; Kawahara et al., 2013). Only uniquely mapped reads were extracted and used for downstream analyses, using gene expression level calculated as reads per kilobase per million reads (RPKM). Counts and RPKM for each gene are given in Supplemental Data set S1.

Cluster analysis

Cluster analysis was performed on leaf transcripts that varied by genotype (WT/*csa*) and/or photoperiod (SD/LD). Clustering was performed on the expression-filtered data set by parameters of “at least 1 observation with abs (Val) ≥ 5.0 ” and “MaxVal – MinVal ≥ 5.0 ” using Gene Cluster version 3.0 software (Hoon et al., 2004). Hierarchical clustering was performed after the data were normalized and the heatmap was drawn using the TreeView software (Keil et al., 2016).

Differential gene expression analysis

DEGs were identified with the R/Bioconductor package “DESeq2” (Love et al., 2014). Genes were considered differentially expressed with a $2\times$ difference in expression ($|\log_2 FC| \geq 1$; false discovery rate [FDR] ≤ 0.05 ; P -value ≤ 0.05). DEGs were determined in day (ZT11, 16:00) and night (ZT23, 04:00) tissues, and DEGs regulated the same way in both samples were considered for subsequent analyses (Supplemental Tables S1 and S2 and Supplemental Data sets S2 and S3). GO analysis was performed by Blast2Go and TopGO (Conesa et al., 2005; Alexa and Rahnenfuhrer, 2010), where significance was set at $P < 0.05$, FDR < 0.05 .

WGCNA

Co-expression of anther DEGs was analyzed by the WGCNA package in R (Langfelder and Horvath, 2008). The gradient method was used to test the independence and the average connectivity of different modules at power values from 1 to 20; the appropriate power value was determined when the degree of independence was 0.8 (power = 16, Supplemental Figure S4B). Genes were then separated into different modules using the WGCNA algorithm (minimum number per module set to 40). Module–trait associations were estimated using the correlation between the ME and the phenotype. The intramodular hub-genes of each module were chosen by external traits, using $GS > 0.2$, $MM > 0.8$, threshold of P -value < 0.05 (Horvath and Dong, 2008). The expression pattern of each module was plotted by R package of “ggplot2” (Wickham, 2016).

RT-qPCR

Total RNA was extracted from anther and flag leaf using Trizol, as above. Concentration of total RNA was measured with the NanoDrop 2000 (Thermo Fisher Waltham, MA, USA). Samples were pretreated with DNase, then RT was performed using the FastKing RT Kit (Tiangen Biotech Co) to synthesize first-stand cDNA from 2 μ g RNA. cDNA was diluted to 100 μ L with DEPC [9]-treated water and 2 μ L of cDNA was used as template for RT-qPCR using QuantiNova SYBR green PCR kit (Qiagen, Hilden, Germany). The PCR reaction procedures were performed on the Bio-Rad CFX96 Real-Time System: 95°C for 2 min for pre-denaturation; followed by 40 cycles of 95°C for 5 s and 60°C for 10 s for two-step amplification. Relative expression to *ACTIN1* was calculated using $2^{-\Delta\Delta Ct}$ methods. Primers used for RT-qPCR are shown in Supplemental Table S9.

Transgenic plant production

ProCSA::CSA-FLAG was created by inserting the CSA promoter (2,199 bp) and cDNA fragment excluding stop codon (1,017 bp) into the *EcoRI* and *BstEII* sites of pCAMBIA1301, then inserting two FLAG-tag fragments into the *BstEII* site. Primers used for vector construction are shown in Supplemental Table S10. For CRISPR/Cas9 mutagenesis, targets were designed using the CRISPR-P 2.0 database (<http://crispr.hzau.edu.cn/cgi-bin/CRISPR2/SCORE>; Supplemental Table S10) and cloned into the plasmid vector pRGE32 according to Xie et al. (2015).

ChIP and quantitative PCR analysis

Rice anthers from transgenic rice plants expressing full-length CSA-FLAG fusion protein were sampled at Stage 12 and fixed in 1% (v/v) formaldehyde (Weng et al., 2018). WT anthers were collected and fixed simultaneously as a negative control. Chromatin was extracted according to Weng et al. (2018) and sonicated for 30 s with a 30-s break at high energy with an ultrasonic disrupter (Diagenode, Bioruptor) for 20–30 rounds, yielding chromatin DNA of 200–500 bp. Immunoprecipitation was performed using the FLAG-TAG antibody (Sigma, St. Louis, MO, USA; F2555). qPCR was performed using primers designed to MYB binding motifs (Supplemental Table S11). *MST8*, a direct down-stream target of CSA, was used as a positive control (Zhang et al., 2010) and *ACTIN1* was used as a negative control.

Dual-LUC assays

Dual-LUC assay methods were modified from a protocol previously reported in *N. benthamiana* plants (Hellens et al., 2005). Full-length CSA cDNA was cloned into pGreenII-0000 plasmid to form the 35S::CSA effector, with a 35S::GFP negative control (Figure 6K). Reporter vectors were generated by inserting the promoters of CSA down-stream candidates into pGreenII-0800 plasmid (Figure 6K). All effector and reporter vectors were transformed into *Agrobacterium tumefaciens* (strain GV3101) with the help of pSoup-P19 plasmid (Li et al., 2014).

Agrobacteria were cultured overnight (~16 h) and collected by centrifugation at 2,500 g for 5 min, then resuspended in MS liquid medium to $OD_{600} = 0.6$, and incubated at room temperature for 3 h after adding MES (pH 5.6) to 10 mM and acetosyringone to 200 μ M final concentration (Li et al., 2014). *Agrobacterium tumefaciens* strains containing effectors and reporters were mixed 4:1 and infiltrated into a young leaf of *N. benthamiana*. After growing for about 48 h under weak light conditions, injected leaves were collected and frozen in liquid nitrogen immediately. LUC and Renilla (REN) activities were measured using the Promega Dual-LUC Reporter Assay Systems kits according to the manufacturer's instructions using a GloMax 20/20 Luminometer (Promega, Madison, WI, USA). Five biological repeats were measured for each sample; differences in expression were assessed using Student's *t* test (Statistical Product and Service Solutions, SPSS version 16.0).

Pollen viability staining

Anthers were randomly collected at Stage 13, then immersed and crushed in 1% I₂-KI solution on glass slides (Zhang and Wilson, 2009). Pollen staining was observed by Nikon ECLIPSE 80i microscope according to the manufacturer's protocol. Fertile pollen rates of nine pollen grains from three plants were calculated after the pictures were captured with appropriate parameters. Significant differences were assessed using Student's *t* test (SPSS version 16.0).

Soluble sugar content and starch content measurement

Soluble sugar content was analyzed using the methods modified from protocol previously reported by Lisec et al. (2006). At Stage 10 of the anther development, 20 mg (fresh weight [FW]) of anther, 50 mg of flag leaf, and 50 mg of lemma/palea were harvested and fixed in liquid nitrogen. Enzyme activities were terminated with methanol. The soluble sugar was extracted by trichloromethane and dried by lyophilization. The dried powder was treated with 25 μ L methoxyamine hydrochloride (20 mg/mL in pyridine solution) and shaken at 30°C for 90 min, after which 40 μ L *N*-methyl-*N*-(trimethylsilyl) trifluoroacetamide was added and allowed to incubate at 37°C for 30 min and 25°C for 120 min. Soluble sugars, including sucrose, glucose, and fructose, were detected using gas chromatography–mass spectrometry (Agilent GC-7890B MS-5977B). Starch content was measured using the standard curve method with multifunctional microplate reader reported by Li and Peng (2018). Significant differences were assessed using Student's *t* test (SPSS version 16.0).

Accession numbers

All the scripts used in this study were uploaded in the GitHub repository: <https://github.com/ljbsk/SHARE/find/DEG-WGCNA-GO>. The datasets presented in this paper can be found in GenBank (<http://www.ncbi.nlm.nih.gov>) under accession number GSE171078. Sequence data from this article can be found in the GenBank data libraries under accession numbers OM515204-OM515212.

Supplemental data

The following materials are available in the online version of this article.

Supplemental Table S1. DEGs in flag leaf samples.

Supplemental Table S2. DEGs in anther samples.

Supplemental Table S3. Numbers of genes in WGCNA co-expression modules.

Supplemental Table S4. Biological process analysis by GO of the MEs in turquoise module and blue module.

Supplemental Table S5. DEGs involved in cell wall modification and actin filament depolymerization in the “*csa*-sterility” DEG set.

Supplemental Table S6. DEGs involved in cell wall development and actin filament organization in the “fertility restoration” DEG set.

Supplemental Table S7. Soluble sugars and starch level profiles in WT and mutants.

Supplemental Table S8. Common DEGs between anthers and flag leaves in *csa*-SD compared with WT-SD.

Supplemental Table S9. List of primers for RT-qPCR analysis and vector construction.

Supplemental Table S10. List of sgRNAs for CRISPR/Cas9 system.

Supplemental Table S11. List of primers used in ChIP-qPCR assay.

Supplemental Figure S1. Sampling points of rice leaves and anthers under LD and SD conditions.

Supplemental Figure S2. Sample clustering of the transcriptomes by replicates in leaves under different conditions.

Supplemental Figure S3. Expression pattern of genes involved in circadian rhythm regulation and photoperiod sensing in WT anthers under SD and LD conditions during the day (ZT11, 16:00) and night (ZT23, 04:00).

Supplemental Figure S4. Quality control of WGCNA analysis of anther DEGs.

Supplemental Figure S5. Gene expression patterns of the co-expression modules.

Supplemental Figure S6. Expression pattern of genes involved in circadian rhythm regulation and photoperiod sensing in the WT and *csa* anthers during the day (ZT11, 16:00) and night (ZT23, 04:00) under SD conditions.

Supplemental Data set S1. Data of all counts and RPKM for each gene.

Supplemental Data set S2. The full results of DEG analyses in the leaves.

Supplemental Data set S3. The full results of DEG analyses in the anthers.

Supplemental Data set S4. Genes in each WGCNA module.

Acknowledgments

We thank Dr. Natalie Betts for providing advice on manuscript preparation. We also thank Ms. Mingjiao Chen and Ms. Xiaofei Chen for their efforts on the rice tissue culture, and Mr. Zhijing Luo, Mr. Zibo Chen, and Mr. Ting Luo for the rice planting in the paddy field.

Funding

This work was supported by grants from the National Natural Science Foundation of China (31970803), China–Germany Mobility Program (M-0141) and the Innovative Research Team, Ministry of Education, and 111 Project (B14016).

Conflict of interest statement. We declare that we have no conflict of interest to this work.

References

Adams S, Manfield I, Stockley P, Carre IA (2015) Revised morning loops of the Arabidopsis circadian clock based on analyses of direct regulatory interactions. *PLoS ONE* 10: e0143943

- Alabadi D, Oyama T, Yanovsky MJ, Harmon FG, Mas P, Kay SA** (2001) Reciprocal regulation between TOC1 and LHY/CCA1 within the Arabidopsis circadian clock. *Science* **293**: 880–883
- Alexa A, Rahnenfuhrer J** (2010) Type package title topGO: enrichment analysis for gene ontology version 2.10.0. DOI: 10.18129/B9.bioc.topGO
- Bihmidine S, Hunter CT 3rd, Johns CE, Koch KE, Braun DM** (2013) Regulation of assimilate import into sink organs: Update on molecular drivers of sink strength. *Front Plant Sci* **4**: 177
- Chen R, Zhao X, Shao Z, Wei Z, Wang Y, Zhu L, Zhao J, Sun M, He R, He G** (2007a) Rice UDP-glucose pyrophosphorylase1 is essential for pollen callose deposition and its cosuppression results in a new type of thermosensitive genic male sterility. *Plant Cell* **19**: 847–861
- Chen T, Teng N, Wu X, Wang Y, Tang W, Samaj J, Baluska F, Lin J** (2007b) Disruption of actin filaments by latrunculin B affects cell wall construction in *Picea meyeri* pollen tube by disturbing vesicle trafficking. *Plant Cell Physiol* **48**: 19–30
- Cheng SH, Zhuang JY, Fan YY, Du JH, Cao LY** (2007) Progress in research and development on hybrid rice: A super-domesticated in China. *Ann Bot* **100**: 959–966
- Chu ZH, Yuan M, Yao LL, Ge XJ, Yuan B, Xu CG, Li XH, Fu BY, Li ZK, Bennetzen JL, et al.** (2006) Promoter mutations of an essential gene for pollen development result in disease resistance in rice. *Gene Dev* **20**: 1250–1255
- Conesa A, Götz S, García-Gómez J, Terol J, Talón M, Robles M** (2005) Sequence analysis Blast 2 GO: A universal tool for annotation, visualization and analysis in functional genomics research. *Bioinformatics* **21**: 3674–3676
- Corbesier L, Vincent C, Jang SH, Fornara F, Fan QZ, Searle I, Giakountis A, Farrona S, Gissot L, Turnbull C, et al.** (2007) FT protein movement contributes to long-distance signaling in floral induction of Arabidopsis. *Science* **316**: 1030–1033
- Cosgrove DJ** (2005) Growth of the plant cell wall. *Nat Rev Mol Cell Biol* **6**: 850–861
- Deng X, An B, Zhong H, Yang J, Kong W, Li Y** (2019) A novel insight into functional divergence of the MST gene family in rice based on comprehensive expression patterns. *Genes* **10**: 239
- Ding JH, Lu Q, Ouyang YD, Mao HL, Zhang PB, Yao JL, Xu CG, Li XH, Xiao JH, Zhang QF** (2012) A long noncoding RNA regulates photoperiod-sensitive male sterility, an essential component of hybrid rice. *Proc Natl Acad Sci USA* **109**: 2654–2659
- Doi K, Izawa T, Fuse T, Yamanouchi U, Kubo T, Shimatani Z, Yano M, Yoshimura A** (2004) Ehd1, a B-type response regulator in rice, confers short-day promotion of flowering and controls FT-like gene expression independently of Hd1. *Genes Dev* **18**: 926–936
- Dunlap JC** (1999) Molecular bases for circadian clocks. *Cell* **96**: 271–290
- Fan YR, Yang JY, Mathioni SM, Yu JS, Shen JQ, Yang XF, Wang L, Zhang QH, Cai ZX, Xu CG, et al.** (2016) PMS1T, producing phased small-interfering RNAs, regulates photoperiod-sensitive male sterility in rice. *Proc Natl Acad Sci USA* **113**: 15144–15149
- Flis A, Sulpice R, Seaton DD, Ivakov AA, Liput M, Abel C, Millar AJ, Stitt M** (2016) Photoperiod-dependent changes in the phase of core clock transcripts and global transcriptional outputs at dawn and dusk in Arabidopsis. *Plant Cell Environ* **39**: 1955–1981
- Fu C, Yang XO, Chen X, Chen W, Ma Y, Hu J, Li S** (2009) OsEF3, a homologous gene of Arabidopsis ELF3, has pleiotropic effects in rice. *Plant Biol (Stuttg)* **11**: 751–757
- Geitmann A, Wojciechowicz K, Cresti M** (1996) Inhibition of intracellular pectin transport in pollen tube by monensin, brefeldin A and cytochalasin D. *Bot Acta* **109**: 373–381
- Hayama R, Coupland G** (2003) Shedding light on the circadian clock and the photoperiodic control of flowering. *Curr Opin Plant Biol* **6**: 13–19
- Hellens RP, Allan AC, Friel EN, Bolitho K, Grafton K, Templeton MD, Karunairetnam S, Gleave AP, Laing WA** (2005) Transient expression vectors for functional genomics, quantification of promoter activity and RNA silencing in plants. *Plant Methods* **1**: 13
- Hoon MJ, Imoto S, Nolan J, Miyano S** (2004) Open source clustering software. *Bioinformatics* **20**: 1453–1454
- Horvath S, Dong J** (2008) Geometric interpretation of gene co-expression network analysis. *PLoS Comput Biol* **4**: e1000117
- Iwamoto M, Higo K, Takano M** (2009) Circadian clock- and phytochrome-regulated Dof-like gene, Rdd1, is associated with grain size in rice. *Plant Cell Environ* **32**: 592–603
- Jiang SY, Cai M, Ramachandran S** (2007) ORYZA SATIVA MYOSIN XI B controls pollen development by photoperiod-sensitive protein localizations. *Dev Biol* **304**: 579–592
- Kawahara Y, Bastide M, Hamilton JP, Kanamori H, McCombie CW, Ouyang S, Schwartz DC, Tanaka T, Wu J, Zhou S, et al.** (2013) Improvement of the *Oryza sativa* Nipponbare reference genome using next generation sequence and optical map data. *Rice* **6**: 4
- Keil C, Leach RW, Faizaan SM, Bezawada S, Parsons L, Baryshnikova A** (2016) Treeview 3 (beta 1)—visualization and analysis of large data matrices [Data set]. Zenodo.
- Langfelder P, Horvath S** (2008) WGCNA: An R package for weighted correlation network analysis. *BMC Bioinformatics* **9**: 559
- Lee E-J, Matsumura Y, Soga K, Hoson T, Koizumi N** (2007) Glycosyl hydrolases of cell wall are induced by sugar starvation in Arabidopsis. *Plant Cell Physiol* **48**: 405–413
- Li D, Yang C, Li X, Gan Q, Zhao X, Zhu L** (2009) Functional characterization of rice OsDof12. *Planta* **229**: 1159–1169
- Li G, Liang W, Zhang X, Ren H, Hu J, Bennett MJ, Zhang D** (2014) Rice actin-binding protein RMD is a key link in the auxin-actin regulatory loop that controls cell growth. *Proc Natl Acad Sci USA* **111**: 10377–10382
- Li YB, Peng B** (2018) Determination of the total starch content of rice seeds. *Biology* **101**: e1010161
- Lisec J, Schauer N, Kopka J, Willmitzer L, Fernie AR** (2006) Gas chromatography mass spectrometry-based metabolite profiling in plants. *Nat Protoc* **1**: 387–396
- Liu L, Zhu Y, Shen LS, Yu H** (2013) Emerging insights into florigen transport. *Curr Opin Plant Biol* **16**: 607–613
- Love MI, Huber W, Anders S** (2014) Moderated estimation of fold change and dispersion for RNA-Seq data with DESeq2. *Genome Biol* **15**: 550
- Malapeira J, Benlloch R, Henriques R, Mas P** (2014) Plant Circadian Network, Springer, New York, pp 333–381
- Mei MH** (1999) Mapping and genetic analysis of the genes for photoperiod-sensitive genic male sterility in rice using the original mutant Nongken 58S. *Crop Sci* **39**: 1711–1715
- Murakami M, Ashikari M, Miura K, Yamashino T, Mizuno T** (2003) The evolutionarily conserved OsPRR quintet: Rice pseudo-response regulators implicated in circadian rhythm. *Plant Cell Physiol* **44**: 1229–1236
- Murakami M, Tago Y, Yamashino T, Mizuno T** (2007) Comparative overviews of clock-associated genes of *Arabidopsis thaliana* and *Oryza sativa*. *Plant Cell Physiol* **48**: 110–121
- Nagel DH, Kay SA** (2013) Complexity in the wiring and regulation of plant circadian networks. *Curr Biol* **23**: 95–96
- Nakamichi N, Kiba T, Henriques R, Mizuno T, Chua NH, Sakakibara H** (2010) PSEUDO-RESPONSE REGULATORS 9, 7, and 5 are transcriptional repressors in the Arabidopsis circadian clock. *Plant Cell* **22**: 594–605
- Oliver SN, Van Dongen JT, Alfred SC, Mamun EA, Zhao XC, Saini HS, Fernandes SF, Blanchard CL, Sutton BG, Geigenberger P, et al.** (2005) Cold-induced repression of the rice anther-specific cell wall invertase gene OSINV4 is correlated with sucrose accumulation and pollen sterility. *Plant Cell Environ* **28**: 1534–1551
- Putterill J, Robson F, Lee K, Simon R, Coupland G** (1995) The CONSTANS gene of Arabidopsis promotes flowering and encodes a protein showing similarities to zinc finger transcription factors. *Cell* **80**: 847–857

- Reboul R, Geserick C, Pabst M, Frey B, Wittmann D, Lütz-Meindl U, Léonard R, Tenhaken R** (2011) Down-regulation of UDP-glucuronic acid biosynthesis leads to swollen plant cell walls and severe developmental defects associated with changes in pectic polysaccharides. *J Biol Chem* **286**: 39982–39992
- Rottmann T, Klebl F, Schneider S, Kischka D, Ruscher D, Sauer N, Stadler R** (2018) Sugar transporter STP7 specificity for L-arabinose and D-xylose contrasts with the typical hexose transporters STP8 and STP12. *Plant Physiol* **176**: 2330–2350
- Ruan YL** (2014) Sucrose metabolism: Gateway to diverse carbon use and sugar signaling. *Annu Rev Plant Biol* **65**: 33–67
- Shi MS** (1985) The discovery and study of the photosensitive recessive male-sterile rice (*Oryza sativa* L. subsp. *japonica*). *Sci Agric Sin* **18**: 44–48
- Siddique S, Sobczak M, Tenhaken R, Grundler FMW, Bohlmann H** (2012) Cell wall ingrowths in nematode induced syncytia require UGD2 and UGD3. *PLoS ONE* **7**: e41515
- Song YH, Smith RW, To BJ, Millar AJ, Imaizumi T** (2012) FKF1 conveys timing information for CONSTANS stabilization in photoperiodic flowering. *Science* **336**: 1045–1049
- Song YH, Ito S, Imaizumi T** (2010) Similarities in the circadian clock and photoperiodism in plants. *Curr Opin Plant Biol* **13**: 594–603
- Sosso D, Luo D, Li QB, Sasse J, Yang J, Gendrot G, Suzuki M, Koch KE, McCarty DR, Chourey PS, et al.** (2015) Seed filling in domesticated maize and rice depends on SWEET-mediated hexose transport. *Nat Genet* **47**: 1489–1493
- Suárez-López P, Wheatley K, Robson F, Onouchi H, Valverde F, Coupland G** (2001) CONSTANS mediates between the circadian clock and the control of flowering in Arabidopsis. *Nature* **410**: 1116–1120
- Sun C, Chen D, Fang J, Wang P, Deng X, Chu C** (2014) Understanding the genetic and epigenetic architecture in complex network of rice flowering pathways. *Protein Cell* **5**: 889–898
- Sun C, Zhang K, Zhou Y, Xiang L, He C, Zhong C, Li K, Wang Q, Yang C, Wang Q, et al.** (2021a) Dual function of clock component OsLHY sets critical day length for photoperiodic flowering in rice. *Plant Biotechnol J* **19**: 1644–1657
- Sun S, Wang D, Li J, Lei Y, Li G, Cai W, Zhao X, Liang W, Zhang D** (2021b) Transcriptome analysis reveals photoperiod-associated genes expressed in rice anthers. *Front Plant Sci* **12**: 621561
- Turgeon R, Wolf S** (2009) Phloem transport: Cellular pathways and molecular trafficking. *Ann Rev Plant Biol* **60**: 207–221
- Vale RD** (2003) The molecular motor toolbox for intracellular transport. *Cell* **112**: 467–480
- Wang D, Li J, Sun L, Hu Y, Yu J, Wang C, Zhang F, Hou H, Liang W, Zhang D** (2021) Two rice MYB transcription factors maintain male fertility in response to photoperiod by modulating sugar partitioning. *New Phytol* **231**: 1612–1629
- Wang K, Singh D, Zeng Z, Coleman SJ, Huang Y, Savich GL, He X, Mieczkowski P, Grimm SA, Perou CM, et al.** (2010) MapSplice: Accurate mapping of RNA-seq reads for splice junction discovery. *Nucleic Acids Res* **38**: e178
- Wang W, Liu Z, Guo Z, Song G, Cheng Q, Jiang D, Zhu Y, Yang D** (2011) Comparative transcriptomes profiling of photoperiod-sensitive male sterile rice Nongken 58S during the male sterility transition between short-day and long-day. *BMC Genomics* **12**: 462
- Weng XY, Zhou SL, Zong W, Ouyang YD** (2018) ChIP assay in rice. *Biology* **101**: e1010135
- Wickham H** (2016) ggplot2: Elegant Graphics for Data Analysis, Springer, Berlin, Germany
- Winter H, Huber SC** (2000) Regulation of sucrose metabolism in higher plants: Localization and regulation of activity of key enzymes. *Crit Rev Biochem Mol Biol* **35**: 253–289
- Xie KB, Minkenberg B, Yang YN** (2015) Boosting CRISPR/Cas9 multiplex editing capability with the endogenous tRNA-processing system. *Proc Natl Acad Sci USA* **112**: 3570–3575
- Yang J, Luo D, Yang B, Frommer WB, Eom JS** (2018) SWEET11 and 15 as key players in seed filling in rice. *New Phytol* **218**: 604–615
- Yang Y, Peng Q, Chen GX, Li XH, Wu CY** (2013) OsELF3 is involved in circadian clock regulation for promoting flowering under long-day conditions in rice. *Mol Plant* **6**: 202–215
- Yano M, Katayose Y, Ashikari M, Yamanouchi U, Monna L, Fuse T, Baba T, Yamamoto K, Umehara Y, Nagamura Y, et al.** (2000) Hd1, a major photoperiod sensitivity quantitative trait locus in rice, is closely related to the Arabidopsis flowering time gene CONSTANS. *Plant Cell Online* **12**: 2473–2484
- Yuan L** (1994) Purification and production of foundation seed of rice PGMS and TGMS lines. *Hybrid Rice* **6**: 1–3
- Zhang D, Wilson ZA** (2009) Stamen specification and anther development in rice. *Chin Sci Bull* **54**: 2342–2353
- Zhang H, Liang W, Yang X, Luo X, Jiang N, Ma H, Zhang D** (2010) Carbon starved anther encodes a MYB domain protein that regulates sugar partitioning required for rice pollen development. *Plant Cell* **22**: 672–689
- Zhang H, Xu CX, He Y, Zong J, Yang XJ, Si HM, Sun ZX, Hu JP, Liang WQ, Zhang DB** (2013) Mutation in CSA creates a new photoperiod-sensitive genic male sterile line applicable for hybrid rice seed production. *Proc Natl Acad Sci USA* **110**: 76–81
- Zhang Q, Shen BZ, Dai XK, Mei MH, Saghai Marofo MA, Li ZB** (1994) Using bulked extremes and recessive class to map genes for photoperiod-sensitive genic male sterility in rice. *Proc Natl Acad Sci USA* **91**: 8675–8679
- Zhou H, Liu Q, Li J, Jiang D, Zhou L, Wu P, Lu S, Li F, Zhu L, Liu Z, et al.** (2012) Photoperiod- and thermo-sensitive genic male sterility in rice are caused by a point mutation in a novel noncoding RNA that produces a small RNA. *Cell Res* **22**: 649–660
- Zhou Y, Liu L, Huang W, Yuan M, Zhou F, Li X, Lin Y** (2014) Overexpression of OsSWEET5 in rice causes growth retardation and precocious senescence. *PLoS ONE* **9**: e94210